Electronic Supplementary Material (ESI) for Soft Matter.

Flow and Aggregation of Rod-Like Proteins in Slit and Cylindrical Pores Coated with Polymer Brushes: Insight from Dissipative Particle Dynamics

Zbyšek Posel,[1,3,*] Martin Svoboda,[2,3] Coray M. Colina,[4] and Martin Lísal[2,3]

January 12, 2017

SUPPLEMENTARY INFORMATION

[1] *Department of Informatics, Faculty of Science, J. E. Purkinje University, Ústí n. Lab., Czech Republic*

[2] *Department of Physics, Faculty of Science, J. E. Purkinje University, Ústí n. Lab., Czech Republic*

[3] *Laboratory of Aerosols Chemistry and Physics, Institute of Chemical Process Fundamentals of the CAS, v. v. i., Prague, Czech Republic*

[4] *Department of Chemistry, University of Florida, Gainesville, FL, USA*

[*] Corresponding author: zbysek.posel@ujep.cz

Mailing address: Department of Informatics, Faculty of Science, J. E. Purkinje University,
Ústí n. Lab., Czech Republic

S1 Dissipative Particle Dynamics

Dissipative Particle Dynamics (DPD) models complex systems (in our case, solvent, proteins, brush chains and confining walls) as a collection of mesoscopic beads that represent lumps of real components, containing several atoms or molecules and/or segments [1]. DPD beads are defined by a mass m_i, position $\boldsymbol{r}_i$, and velocity $\boldsymbol{v}_i$, and interact with each other via a pairwise, two-body, short-ranged force $\boldsymbol{f}$ that is written as the sum of a conservative force $\boldsymbol{f}^C$, dissipative force $\boldsymbol{f}^D$, and random force $\boldsymbol{f}^R$:

$$\boldsymbol{f}_{ij} = \boldsymbol{f}_{ij}^C + \boldsymbol{f}_{ij}^D + \boldsymbol{f}_{ij}^R \tag{S1}$$

The conservative force typically includes a bead-bead force acting between two beads i and j, and a spring force acting between adjacent beads in a system's specie. If necessary, a bending force depending on the valence angle between three consecutive beads can be added to increase the stiffness of a system's specie. The $\boldsymbol{f}^C$ is defined as a negative derivative of coarse-grained potentials u^{CG}:

$$\boldsymbol{f}^C = -\nabla_r u^{CG} \tag{S2}$$

Conservative interactions between DPD beads are typically described by a soft-sphere repulsive potential

$$u_{ij}^{CG,b} = \frac{a_{ij}}{2} r_c \omega^C \left(r_{ij} \right) \tag{S3}$$

where a_{ij} is the maximum repulsion between two beads i and j, r_c is the cut-off radius, $\boldsymbol{r}_{ij} = \boldsymbol{r}_i - \boldsymbol{r}_j$ is the separation vector between two beads i and j, $r_{ij} = |\boldsymbol{r}_{ij}|$, and

$$\omega^C(r) = \begin{cases} \left(1 - \frac{r}{r_c}\right)^2 & r < r_c \\ 0 & r \geq r_c \end{cases} \tag{S4}$$

Groot and Warren [1] established a link between a_{ij} and the Flory-Huggins (FH) interaction parameter, χ_{ij}, [2] by mapping the DPD model onto the FH model. Imposing correspondence between the free-energy of the DPD and the FH models, they obtained a simple linear relationship between a_{ij} and χ_{ij}:

$$\chi_{ij} = 2C\rho r_c^3 \left(a_{ij} - \frac{a_{ii} + a_{jj}}{2} \right) \frac{r_c}{kT} \tag{S5}$$

where ρ is the system particle density and C is a constant depending on ρ. Using the equation of state for the soft repulsive DPD fluid together with the compressibility value for ambient water, and assuming $a_{ii} = a_{jj}$, Groot and Warren obtained an expression for like-repulsive parameters

$$\frac{a_{ii} r_c}{kT} \equiv \frac{a_{jj} r_c}{kT} = \frac{75}{\rho r_c^3} \tag{S6}$$

They further reported the linear relationships between unlike-repulsive parameters a_{ij} and χ_{ij} which is for $\rho r_c^3 = 3$ used in this work

$$\frac{\Delta a_{ij} r_c}{kT} \simeq 3.3 \chi_{ij} \tag{S7}$$

where $\Delta a_{ij} = a_{ij} - a_{ii}$.

The dissipative and random forces $\boldsymbol{f}_{ij}^D$ and $\boldsymbol{f}_{ij}^R$ are given by

$$\boldsymbol{f}_{ij}^D = -\gamma_{ij} \omega^D \left(r_{ij}\right) \left(\frac{\boldsymbol{r}_{ij}}{r_{ij}} \cdot \boldsymbol{v}_{ij} \right) \frac{\boldsymbol{r}_{ij}}{r_{ij}} \tag{S8}$$

$$\boldsymbol{f}_{ij}^R = \sigma_{ij} \omega^R \left(r_{ij}\right) \frac{\zeta_{ij}}{\sqrt{\Delta t}} \frac{\boldsymbol{r}_{ij}}{r_{ij}} \tag{S9}$$

where $\omega^D(r)$ and $\omega^R(r)$ are weight functions, that vanish for $r \geq r_c$, γ_{ij} is the friction coefficient, σ_{ij} is the noise amplitude, $\boldsymbol{v}_{ij} = \boldsymbol{v}_i - \boldsymbol{v}_j$, ζ_{ij} is the Gaussian random number with zero mean and unit variance that is chosen independently for each pair of interacting beads, and Δt is the time step.

Español and Warren showed [3] that the system samples the canonical ensemble and obeys the fluctuation-dissipation theorem if the following relationship holds:

$$\sigma_{ij}^2 \left[\omega^R \left(r_{ij}\right)\right]^2 = 2\gamma_{ij} \omega^D \left(r_{ij}\right) kT \tag{S10}$$

where k is the Boltzmann constant and T is the temperature. $\omega^D(r_{ij})$ and $\omega^R(r_{ij})$ are typically chosen [1] as

$$\omega^D \left(r_{ij}\right) = \left[\omega^R \left(r_{ij}\right)\right]^2 = \begin{cases} \left(1 - \frac{r_{ij}}{r_c}\right)^2 & r_{ij} < r_c \\ 0 & r_{ij} \geq r_c \end{cases} \tag{S11}$$

The pressure-driven (Poiseuille) flow can be generated by adding the external force on each fluid particle, $\boldsymbol{f}^e$, which acts in the flow direction; in the x-direction in our case, i.e., $\boldsymbol{f}^e = (f^e, 0, 0)$ [4]. The evolution of DPD beads in time t is governed by the equations of motion

$$\begin{aligned}\frac{\mathrm{d}\boldsymbol{r}_i}{\mathrm{d}t} &= \boldsymbol{v}_i\left(t\right) \\ m_i\frac{\mathrm{d}\boldsymbol{v}_i}{\mathrm{d}t} &= \boldsymbol{f}_i\left(t\right)+\boldsymbol{f}_i^e=\sum_{i\neq j}\left(\boldsymbol{f}_{ij}^C+\boldsymbol{f}_{ij}^D+\boldsymbol{f}_{ij}^R\right)+\boldsymbol{f}_i^e\end{aligned} \tag{S12}$$

DPD is known to have a low Schmidt number [1] and its capability to model dynamics of polymer solutions has been questioned since in the polymer solutions the hydrodynamic interactions between the chain beads become important [5]. Several authors have proposed modifications of DPD that yield a higher Schmidt number [5, 6, 7]. Laradji and his colleagues have analysed potential influence of a low Schmidt number on the dynamics of polymer solutions within DPD. They found that the dynamics of polymer solutions obey the Zimm model. The Zimm model takes into account hydrodynamic interactions through the use of the Navier-Stokes equations for describing the hydrodynamics of solvents and further employs the Oseen tensor to account for the hydrodynamic interaction between chain beads [8]. Laradji and his colleagues concluded that the use of soft repulsive interaction along with a low Schmidt number do not produce noticeable problems for simulations of the equilibrium and out-of-equilibrium dynamics of polymer solutions by DPD [9, 10]. In addition, as noted by Peters [11], the Schmidt number in a coarse-grain model is in fact ill-defined, since in the Schmidt number, the diffusivity of the solvent particles corresponds to the diffusion coefficient of a single particle and not to coarse-grain fluid elements.

For confined polymeric systems, modelling of walls within DPD is not straightforward, see e.g. Refs. [12, 13, 14]. The soft repulsion between DPD particles cannot prevent fluid particles from penetrating surface boundaries, and thus extra effort is needed to impose the no-slip (or partial slip) wall boundary conditions. A well-accepted approach represents a solid surface by frozen particles with a density equal to the fluid density [15]. Fluid and solid particles then preserve their separation through the use of proper reflections when fluid beads are about to cross the given position of the solid surface [16]. In our DPD simulations, confining walls were formed by frozen DPD beads with a density corresponding to the fluid density. The soft repulsion between DPD particles cannot prevent the fluid from penetrating the walls. We thus separated the fluid and wall domains by a reflecting surface and imposed bounce-back reflections when fluid beads are about to cross the solid surface, see Fig. S1. The bounce-back reflection scheme suppresses unphysical fluctuations in the fluid density close the wall and imposes no-slip boundary conditions, i.e., at a solid boundary, the fluid beads have zero velocity relative to the boundary [12, 16].

S2 Additional Results

Figure S1: The schematic representation of the bounce-back reflection scheme for (a) slit- and (b) cylindrical-pore geometries whereas the velocities of the reflected fluid bead are reversed in all dimensions.

Figure S2: (a) The perpendicular radius of the gyration of the brush chains, $R^{P}_{g,\perp}$, in the coated slit pore as a function of the brush-chain length, N_P; good solvent conditions and the grafting density $\sigma_s = 0.5$. (b) The perpendicular radius of the gyration of the brush chains, $R^{P}_{g,\perp}$, in the coated cylindrical pore as a function of the grafting density, σ_c; good solvent conditions and the brush-chain length $N_P = 30$. The dash lines correspond to the scaling given by Alexander-de Gennes' polymer blob model for the semi-dilute brush regime [17, 18, 19]. In figure portion b, the dotted line indicates the value of $R^{P}_{g,\perp}$ for $N_P = 30$ in the coated slit pore with $\sigma_s = 0.5$ and intersection point denoted by star then defines the equivalent grafting density $\sigma_c = 0.325$ in the coated cylindrical pore.

Figure S3: The end-to-end distance, R_e, and the radius of the gyration, R_g, of a polymer chain of a length $N = 30$ in a solvent as a function of the solvent quality, $\Delta a r_c / (kT)$; r_c is the cut-off radius, k is the Boltzmann constant and T is the temperature. The dotted lines serve as a guide to the eye.

Figure S4: The snapshots of proteins in (a, b) the slit and (c, d) cylindrical pores without the polymer brushes. The left column is for the systems under equilibrium conditions while the right column is for the systems in the presence of a flow. Each figure portion displays both a side view (top) and front view (bottom) of the system. The solvent beads are not shown for the sake of clarity.

Figure S5: The number distribution function, F_N, of the aggregation numbers, N_c, for proteins in (a, b) the slit and (c, d) cylindrical pores without the polymer brushes. The left column is for the systems under equilibrium conditions while the right column is for the systems in the presence of a flow.

Figure S6: The distribution of the components of protein's radius of the gyration along the slit pore (left column) and cylindrical pore (right column) without the polymer brushes. The dashed lines represent the systems under equilibrium conditions while solid lines denote the systems in the presence of a flow.

Figure S7: The number distribution function, F_N, of the aggregation numbers, N_c, for proteins in the coated (a, b) slit and (c, d) cylindrical pores in the case of poor solvent conditions (open pore state, $\Delta a = 15$). The left column is for the systems in equilibrium while the right column is for the systems in the presence of a flow.

Figure S8: The distribution of the components of protein's radius of the gyration along the coated slit pore (left column) and coated cylindrical pore (right column) in the case of poor solvent conditions (open pore state, $\Delta a = 15$). The dashed lines represent the systems in equilibrium while solid lines denote the systems in the presence of a flow.

Figure S9: The number distribution function, F_N, of the aggregation numbers, N_c, for proteins in the coated (a, b) slit and (c, d) cylindrical pores in the case of good solvent conditions (closed pore space, $\Delta a = -10$). The left column is for the systems in equilibrium while the right column is for the systems in the presence of a flow.

Figure S10: The distribution of the components of protein's radius of the gyration along the coated slit pore (left column) and coated cylindrical pore (right column) in the case of good solvent conditions (closed pore space, $\Delta a = -10$). The dashed lines represent the systems in equilibrium while solid lines denote the systems in the presence of a flow.

Figure S11: The number distribution function, F_N, of the aggregation numbers, N_c, for proteins in the coated (a, b) slit and (c, d) cylindrical pores in the case of the crossover pore state ($\Delta a_c \simeq 3.7$ for the slit pore and $\Delta a_c \simeq 3.4$ for the cylindrical pore). The left column is for the systems in equilibrium while the right column is for the systems in the presence of a flow.

Figure S12: The distribution of the components of protein's radius of the gyration along the coated slit pore (left column) and coated cylindrical pore (right column) in the case of the crossover pore state ($\Delta a_c \simeq 3.7$ for the slit pore and $\Delta a_c \simeq 3.4$ for the cylindrical pore). The dashed lines represent the systems in equilibrium while solid lines denote the systems in the presence of a flow.

S3 Video Files

UncoatedSlitNoFlow: A video file illustrating protein dynamics in the uncoated slit pore at equilibrium conditions. The solvent beads are suppressed and the brush chains are transparent for the sake of clarity.

UncoatedCylinderNoFlow: A video file illustrating protein dynamics in the uncoated cylindrical pore at equilibrium conditions. The solvent beads are suppressed and the brush chains are transparent for the sake of clarity.

UncoatedSlitFlow: A video file illustrating protein dynamics in the uncoated slit pore under flow. The solvent beads are suppressed and the brush chains are transparent for the sake of clarity.

UncoatedCylinderFlow: A video file illustrating protein dynamics in the uncoated cylindrical pore under flow. The solvent beads are suppressed and the brush chains are transparent for the sake of clarity.

CoatedSlitOpenStateNoFlow: A video file illustrating protein dynamics in the coated slit pore in the open pore state at equilibrium conditions. The solvent beads are suppressed and the brush chains are transparent for the sake of clarity.

CoatedCylinderOpenStateNoFlow: A video file illustrating protein dynamics in the coated cylindrical pore in the open pore state at equilibrium conditions. The solvent beads are suppressed and the brush chains are transparent for the sake of clarity.

CoatedSlitOpenStateFlow: A video file illustrating protein dynamics in the coated slit pore in the open pore state under flow. The solvent beads are suppressed and the brush chains are transparent for the sake of clarity.

CoatedCylinderOpenStateFlow: A video file illustrating protein dynamics in the coated cylindrical pore in the open pore state under flow. The solvent beads are suppressed and the brush chains are transparent for the sake of clarity.

CoatedSlitClosedStateNoFlow: A video file illustrating protein dynamics in the coated slit pore in the closed pore state at equilibrium conditions. The solvent beads are suppressed and the brush chains are transparent for the sake of clarity.

CoatedCylinderClosedStateNoFlow: A video file illustrating protein dynamics in the coated cylindrical pore in the closed pore state at equilibrium conditions. The solvent beads are suppressed and the brush chains are transparent for the sake of clarity.

CoatedSlitClosedStateFlow: A video file illustrating protein dynamics in the coated slit pore in the closed pore state under flow. The solvent beads are suppressed and the brush chains are transparent for the sake of clarity.

CoatedCylinderClosedStateFlow: A video file illustrating protein dynamics in the coated cylindrical pore in the closed pore state under flow. The solvent beads are suppressed and the brush chains are transparent for the sake of clarity.

CoatedSlitCrossoverStateNoFlow: A video file illustrating protein dynamics in the coated slit pore in the crossover pore state at equilibrium conditions. The solvent beads are suppressed and the brush chains are transparent for the sake of clarity.

CoatedCylinderCrossoverStateNoFlow: A video file illustrating protein dynamics in the coated cylindrical pore in the crossover pore state at equilibrium conditions. The solvent beads are suppressed and the brush chains are transparent for the sake of clarity.

CoatedSlitCrossoverStateFlow: A video file illustrating protein dynamics in the coated slit pore in the crossover pore state under flow. The solvent beads are suppressed and the brush chains are transparent for the sake of clarity.

CoatedCylinderCrossoverStateFlow: A video file illustrating protein dynamics in the coated cylindrical pore in the crossover pore state under flow. The solvent beads are suppressed and the brush chains are transparent for the sake of clarity.

References

[1] R. D. Groot and P. B. Warren, *J. Chem. Phys.*, 1997, **107**, 4423-4435.

[2] P. J. Flory, *Principles of Polymer Chemistry*, Cornell University Press, New York, NY, 1953.

[3] P. Español and P. B. Warren, *Europhys. Lett.*, 1995, **30**, 191-196.

[4] J. A. Millan, W. Jiang, M. Laradji and Y. Wang, *J. Chem. Phys.*, 2007, **126**, 124905.

[5] V. Symeonidis, G. E. Karniadakis and B. Caswell, *J. Chem. Phys.*, 2006, **125**, 184902.

[6] Z. Li and G. Drazer, *Phys. Fluids*, 2008, **20**, 103601.

[7] R. C. Krafnick and A. E. García, *J. Chem. Phys.*, 2015, **143**, 243106.

[8] B. H. Zimm, *J. Chem. Phys.*, 1956, **24**, 269-278.

[9] Z. Li, Y. Li, Y. Wang, Z. Sun and L. An, *Macromolecules*, 2010, **43**, 5896-5903.

[10] W. Jiang, J. Huang, Y. Wang and M. Laradji, *J. Chem. Phys.*, 2007, **126**, 044901.

[11] E. A. J. F. Peters, *Europhys. Lett.*, 2004, **66**, 311-317.

[12] I. V. Pivkin and G. E. Karniadakis, *J. Comput. Phys.*, 2005, **207**, 114-128.

[13] P. Petrus, M. Lísal and J. K. Brennan, *Langmuir*, 2010, **26**, 3695-3709.

[14] P. Petrus, M. Lísal and J. K. Brennan, *Langmuir*, 2010, **26**, 14680-14693.

[15] N. A. Gatsonis, R. Potami and J. Yang, *J. Comput. Phys.*, 2014, **256**, 441-464.

[16] M. A. Seaton, R. L. Anderson, S. Metz and W. Smith, *Molec. Simul.*, 2013, **39**, 796-821.

[17] S. Alexander, *J. Phys. (Paris)*, 1977, **38**, 983-987.

[18] P.-G. de Gennes, *J. Phys. (Paris)*, 1976, **37**, 1443-1452.

[19] P.-G. de Gennes, *Macromolecules*, 1980, **13**, 1069-1075.

Fig. S1 (Posel et al.)

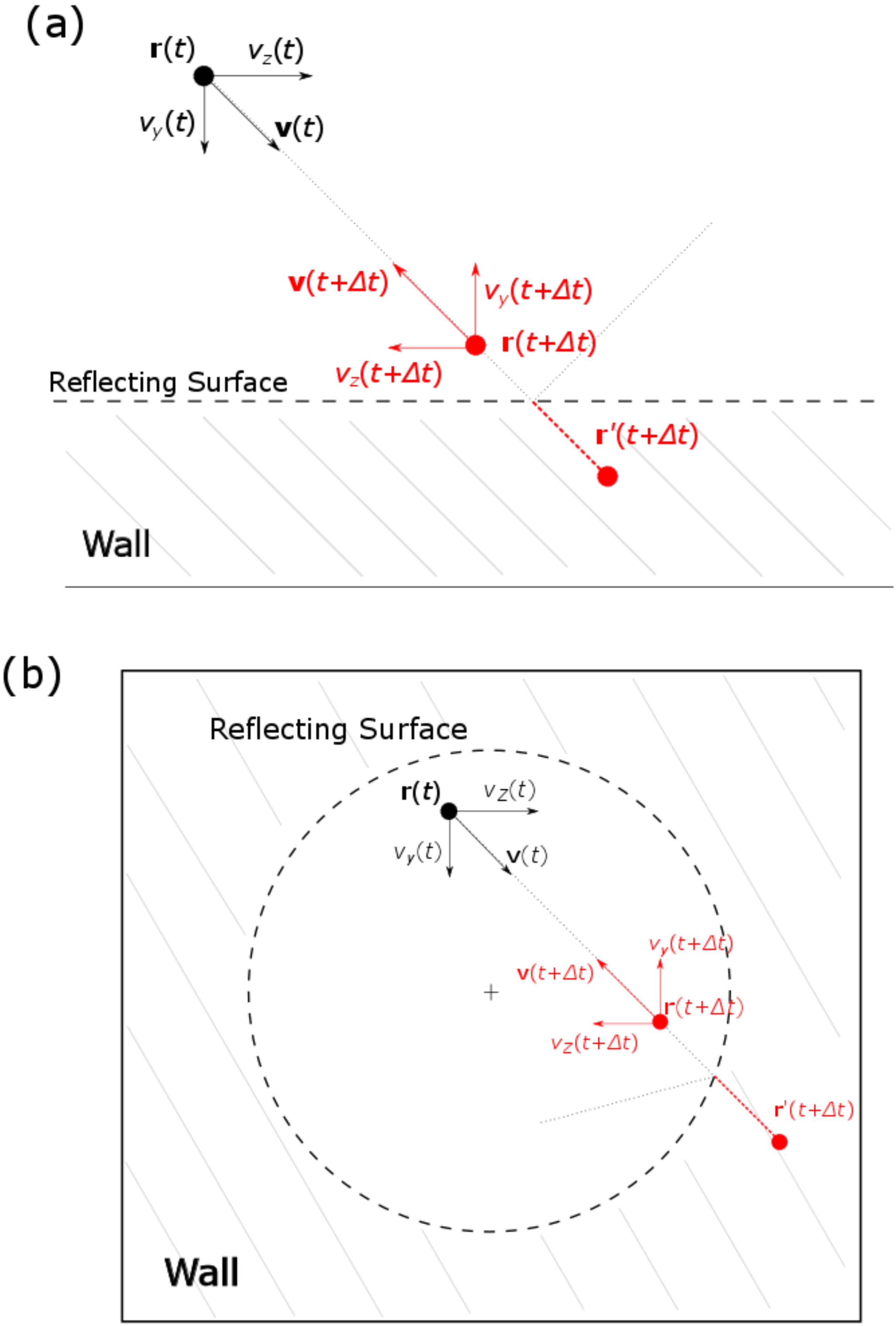

Fig. S2 (Posel et al.)

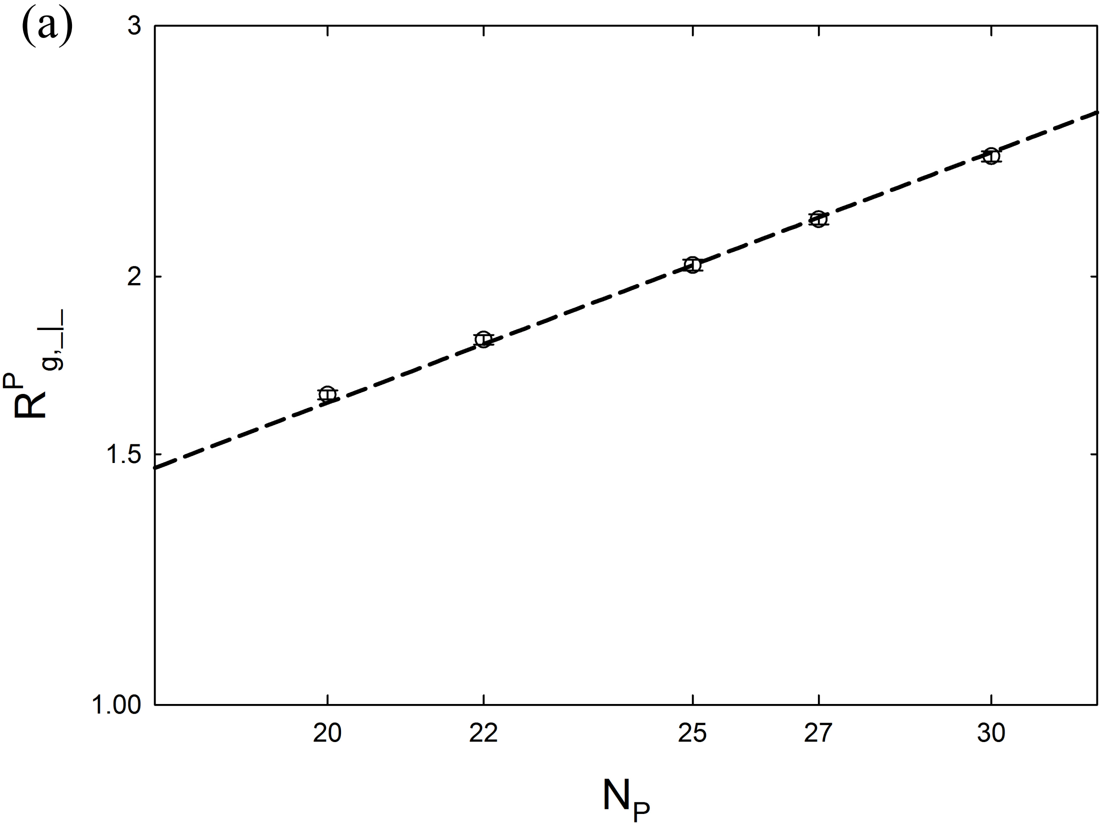

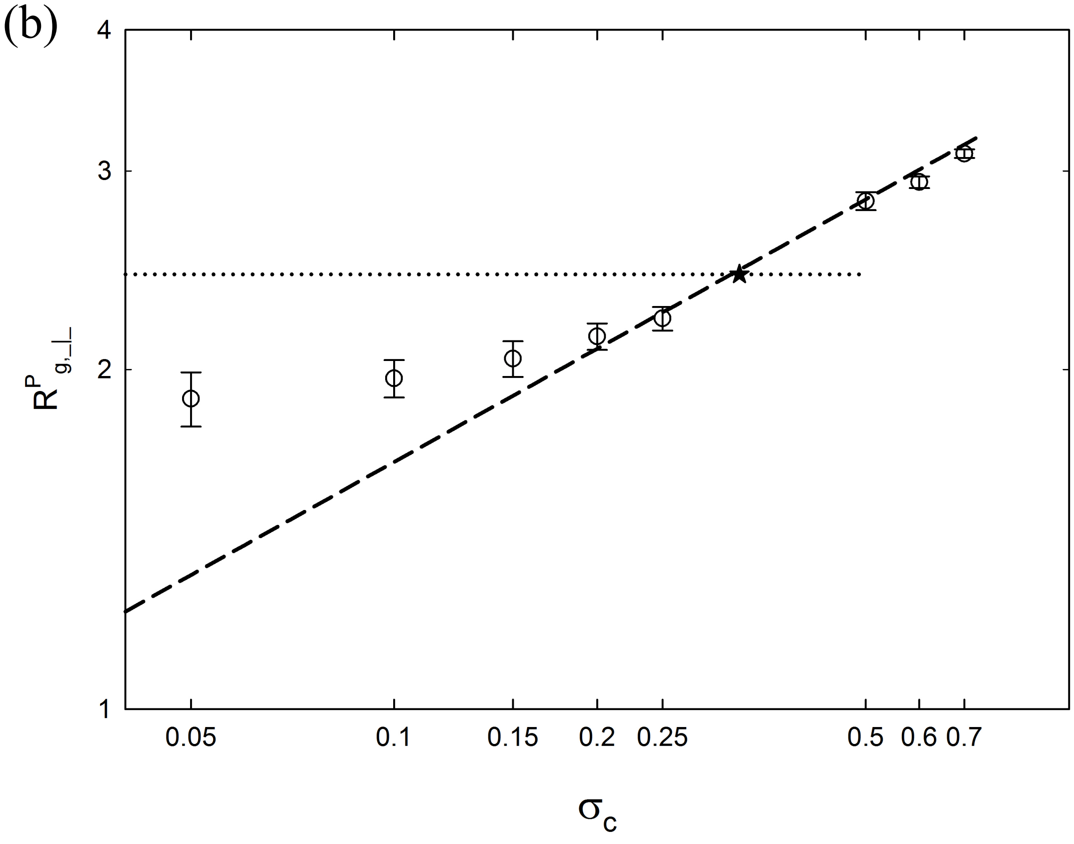

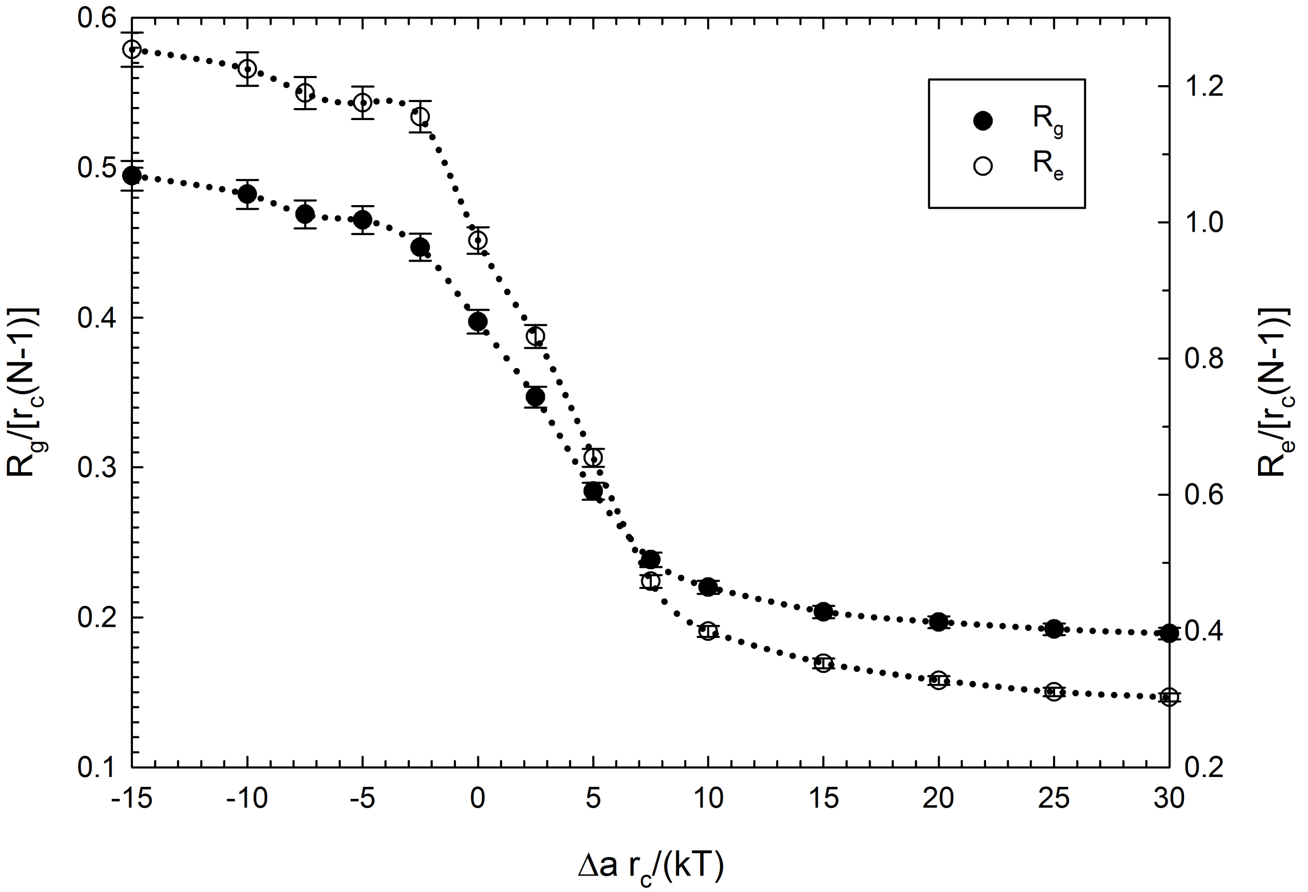
$R_g/[r_c(N-1)]$
0.6
0.5
0.4
0.3
0.2
0.1
$R_e/[r_c(N-1)]$
1.2
1.0
0.8
0.6
0.4
0.2
-15
-10
-5
0
5
10
15
20
25
30
$\Delta a\ r_c/(kT)$
● R_g
○ R_e

Fig. S4 (Posel et al.)

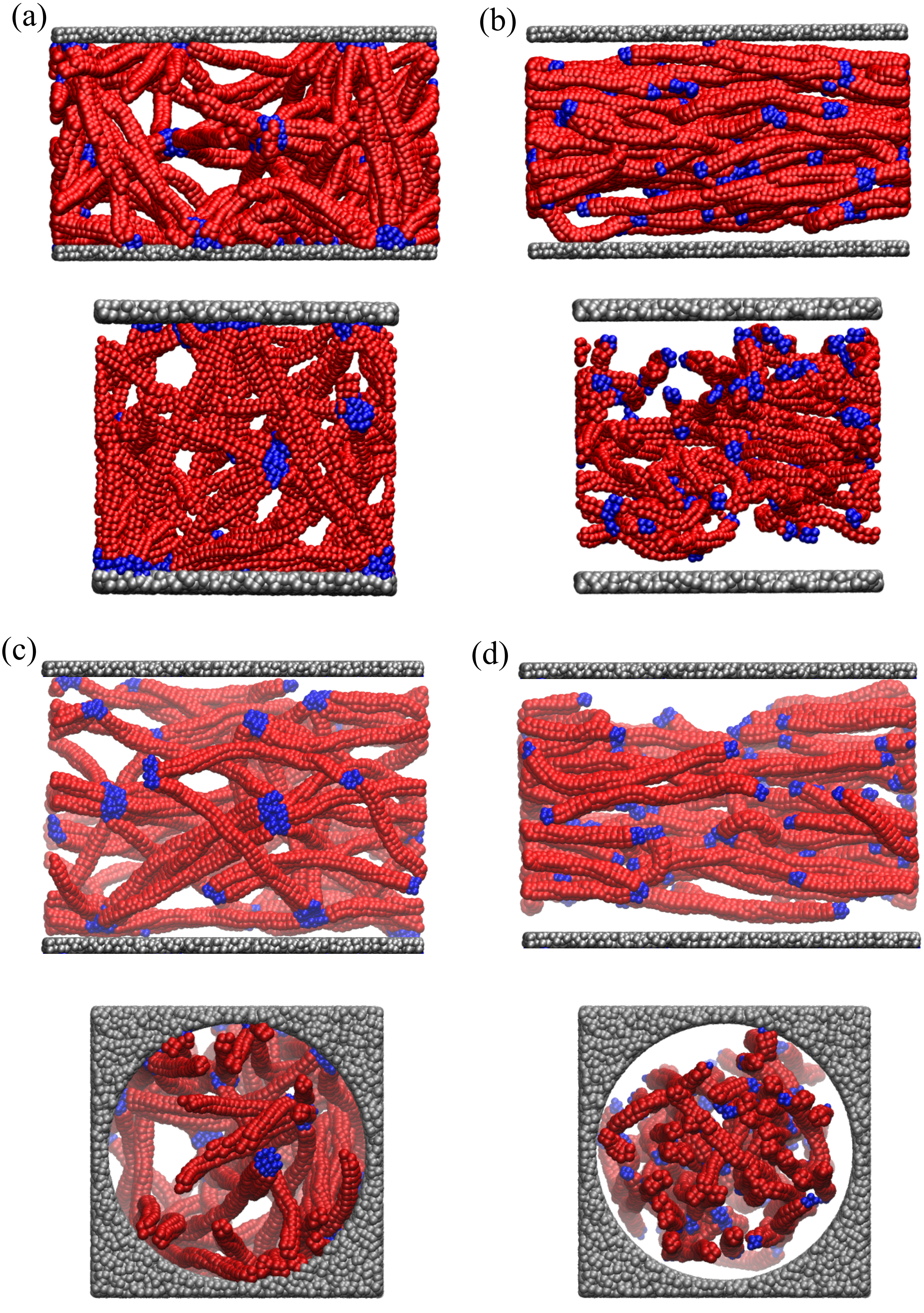

Fig. S5 (Posel et al.)

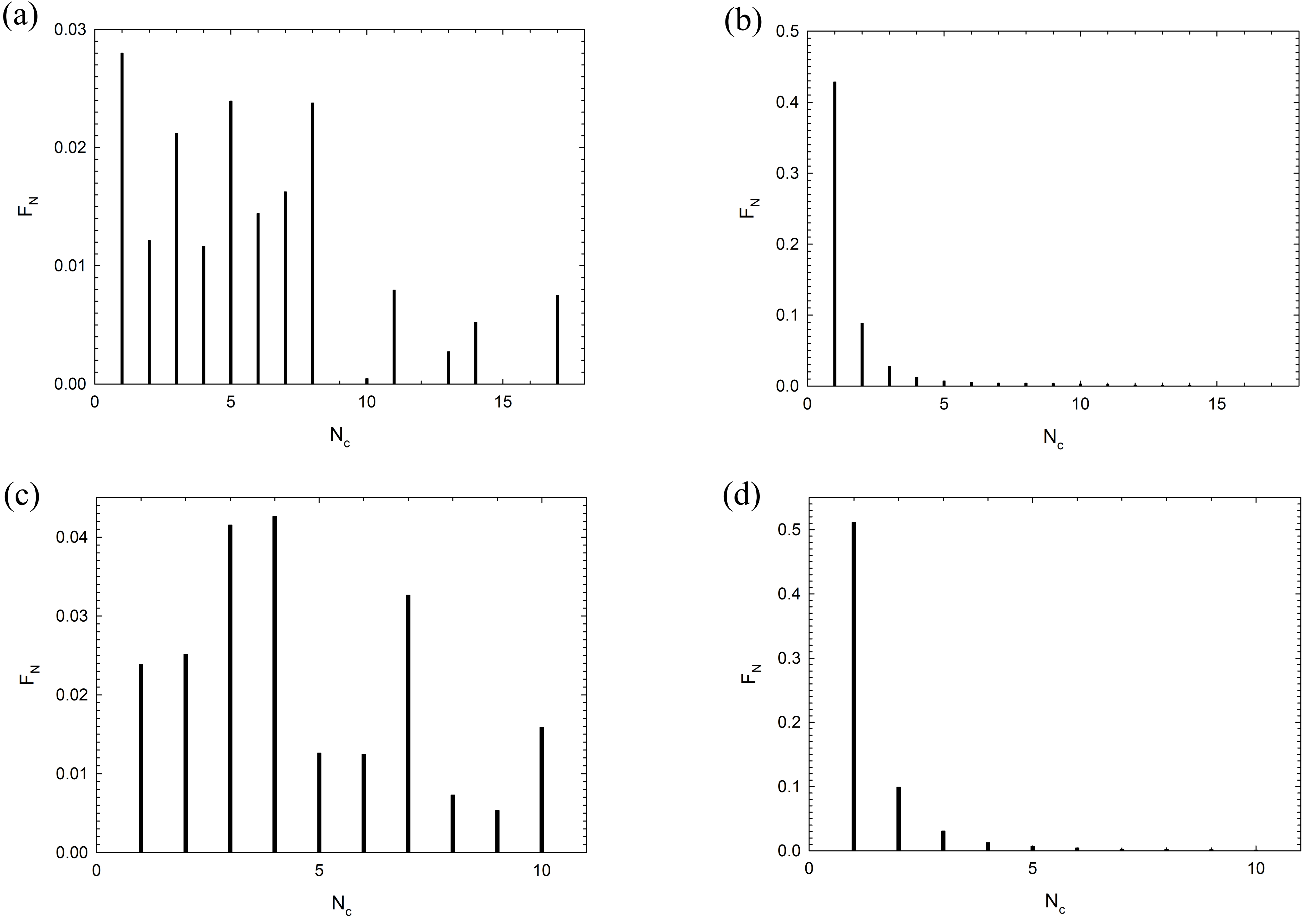

Fig. S6 (Posel et al.)

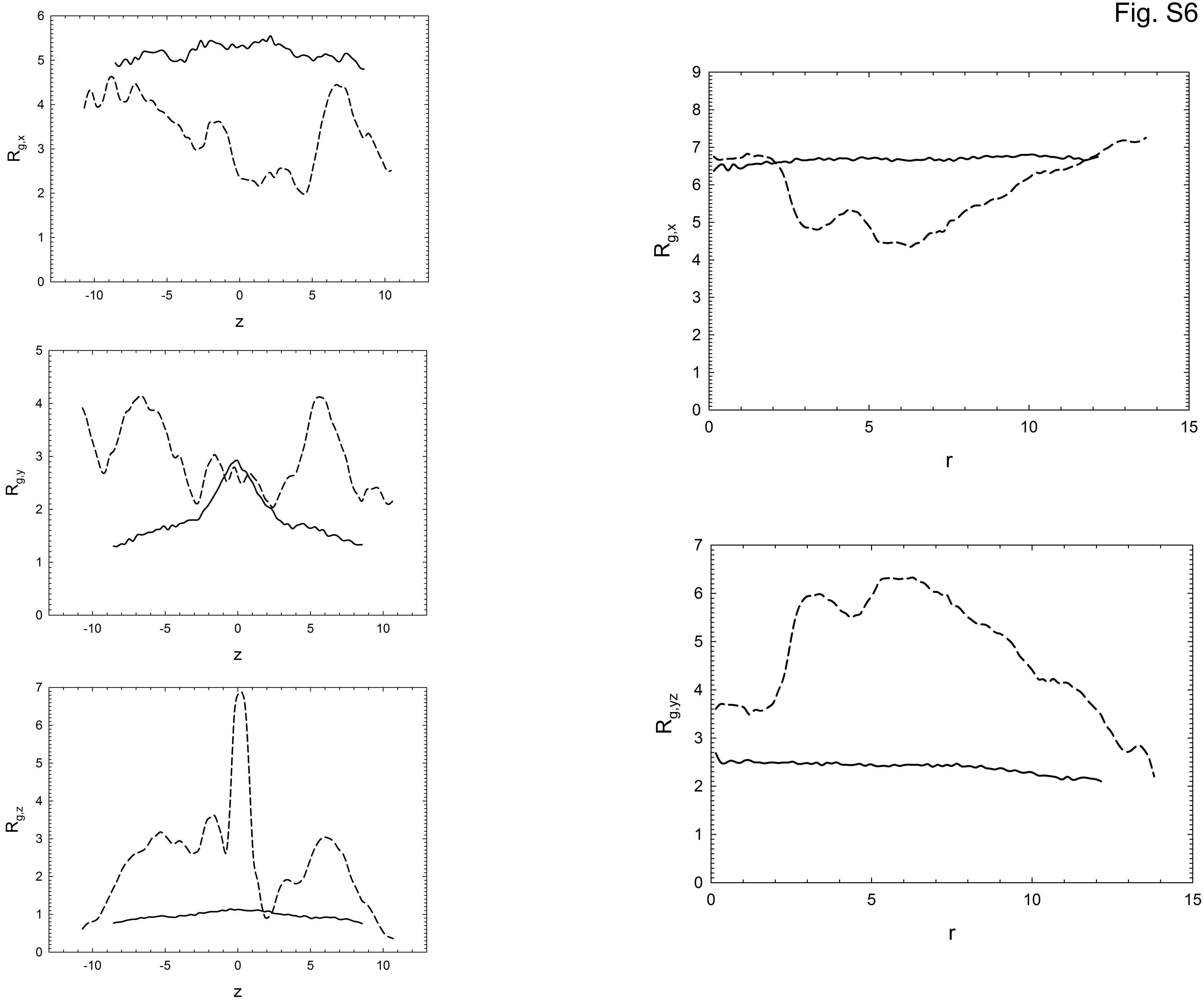

Fig. S7 (Posel et al.)

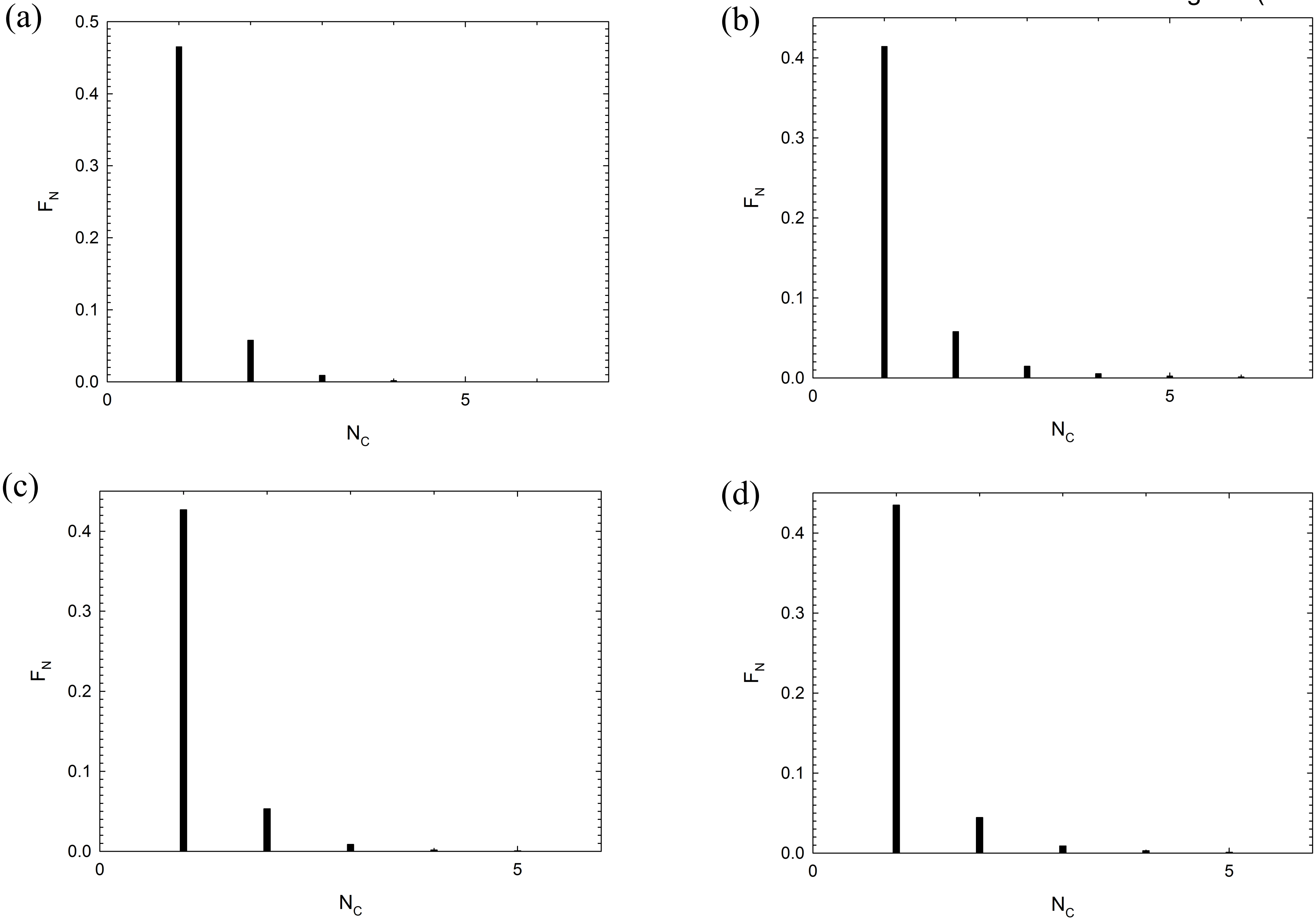

Fig. S8 (Posel et al.)

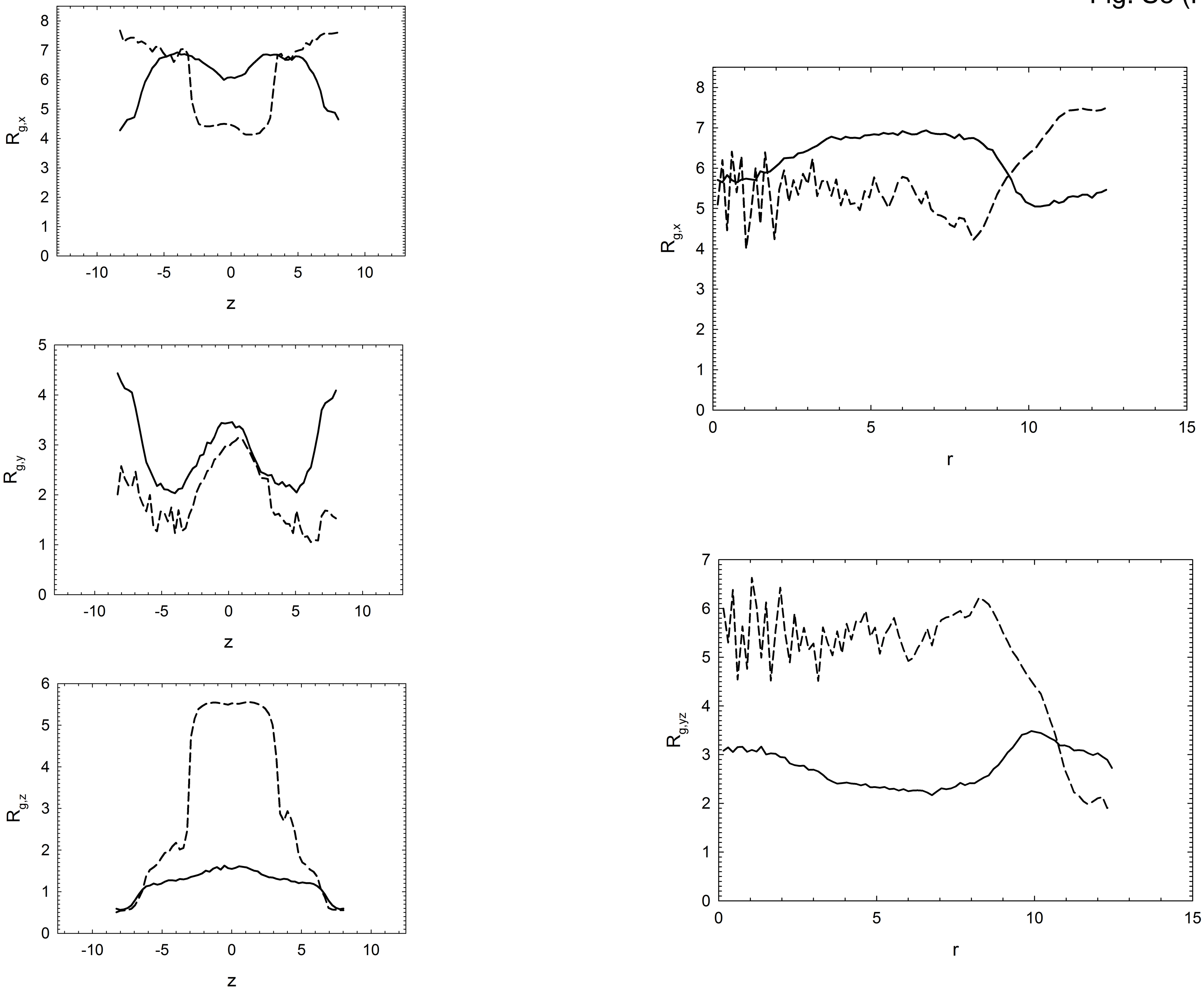

Fig. S9 (Posel et al.)

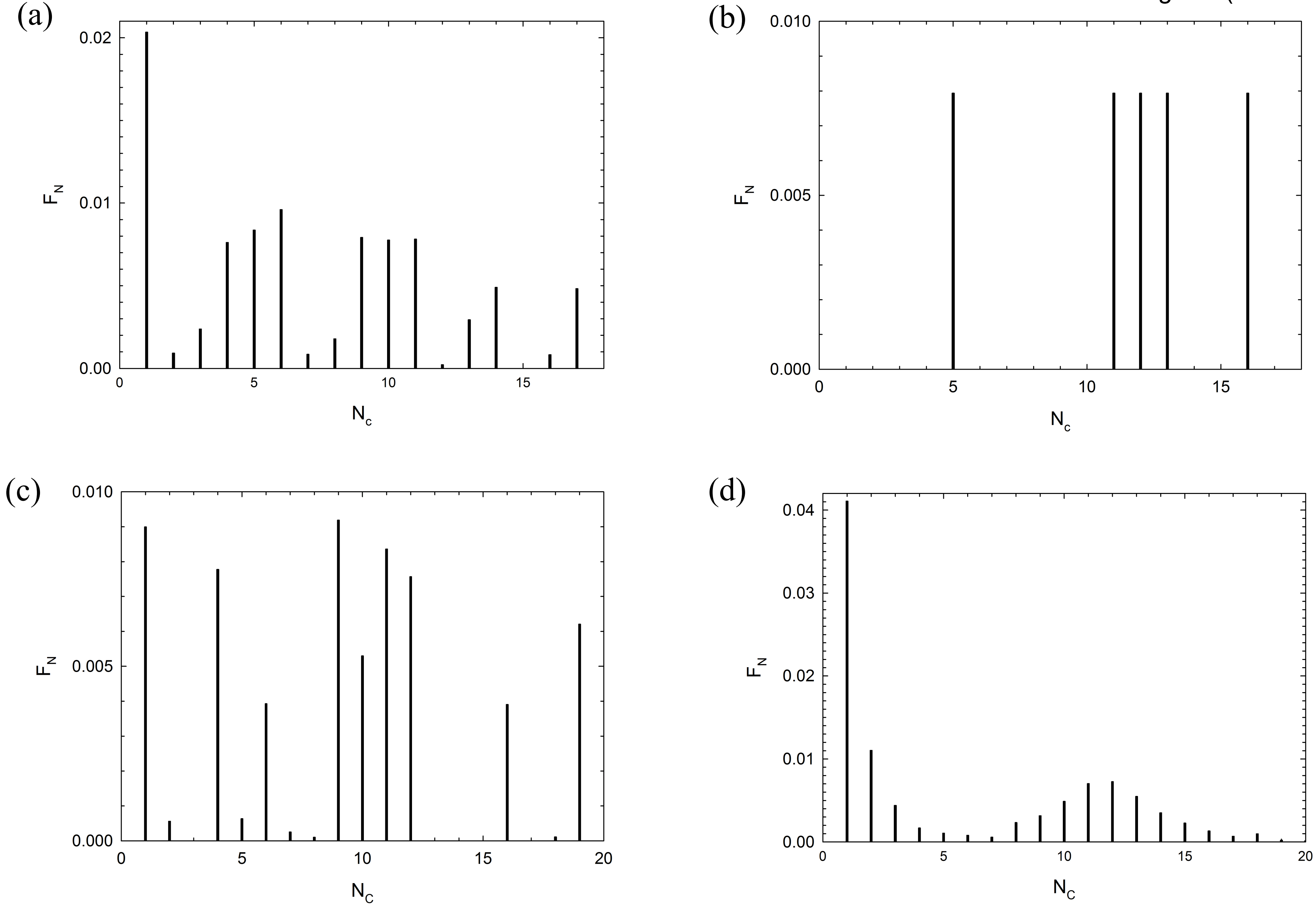

Fig. S10 (Posel et al.)

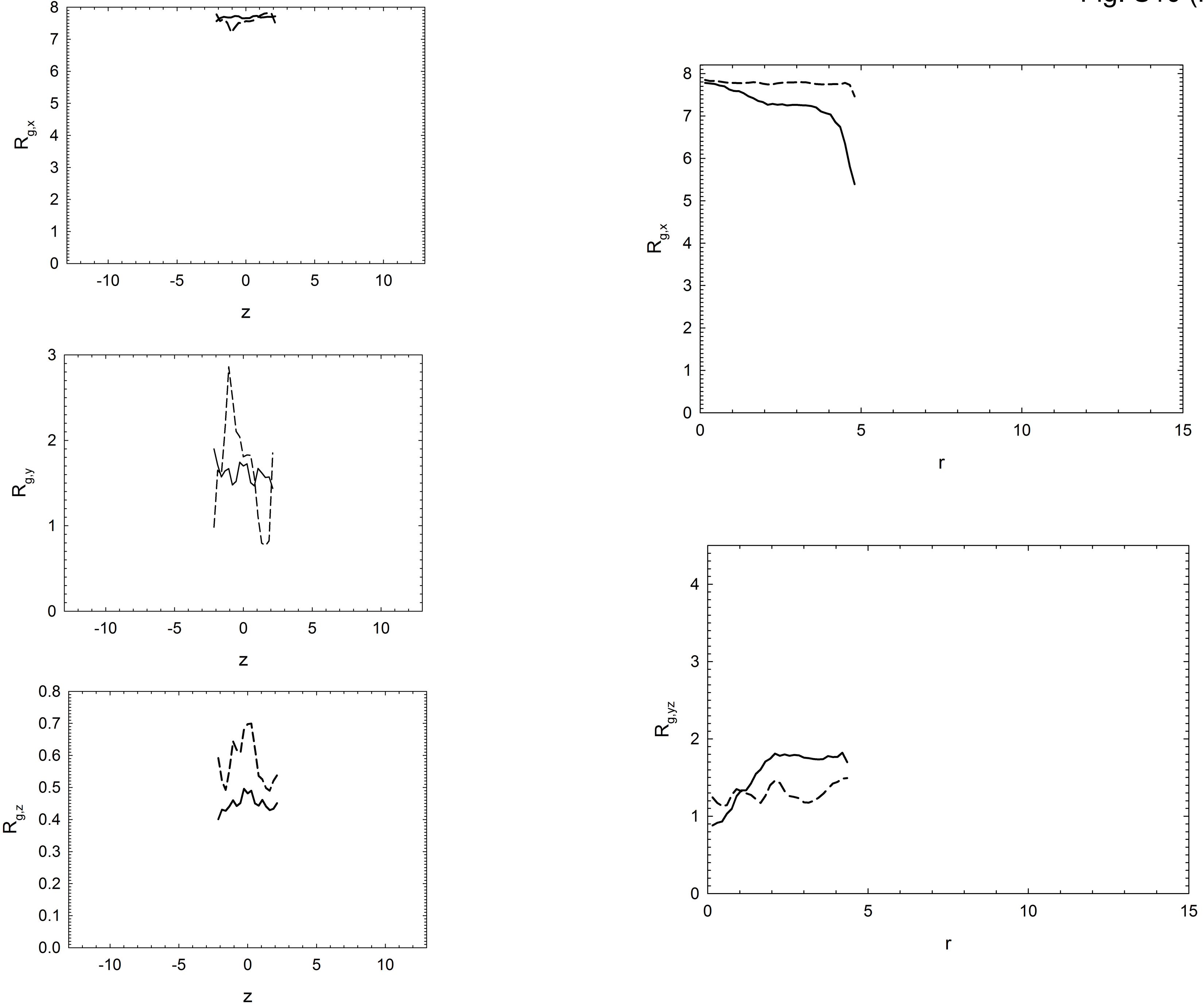

Fig. S11 (Posel et al.)

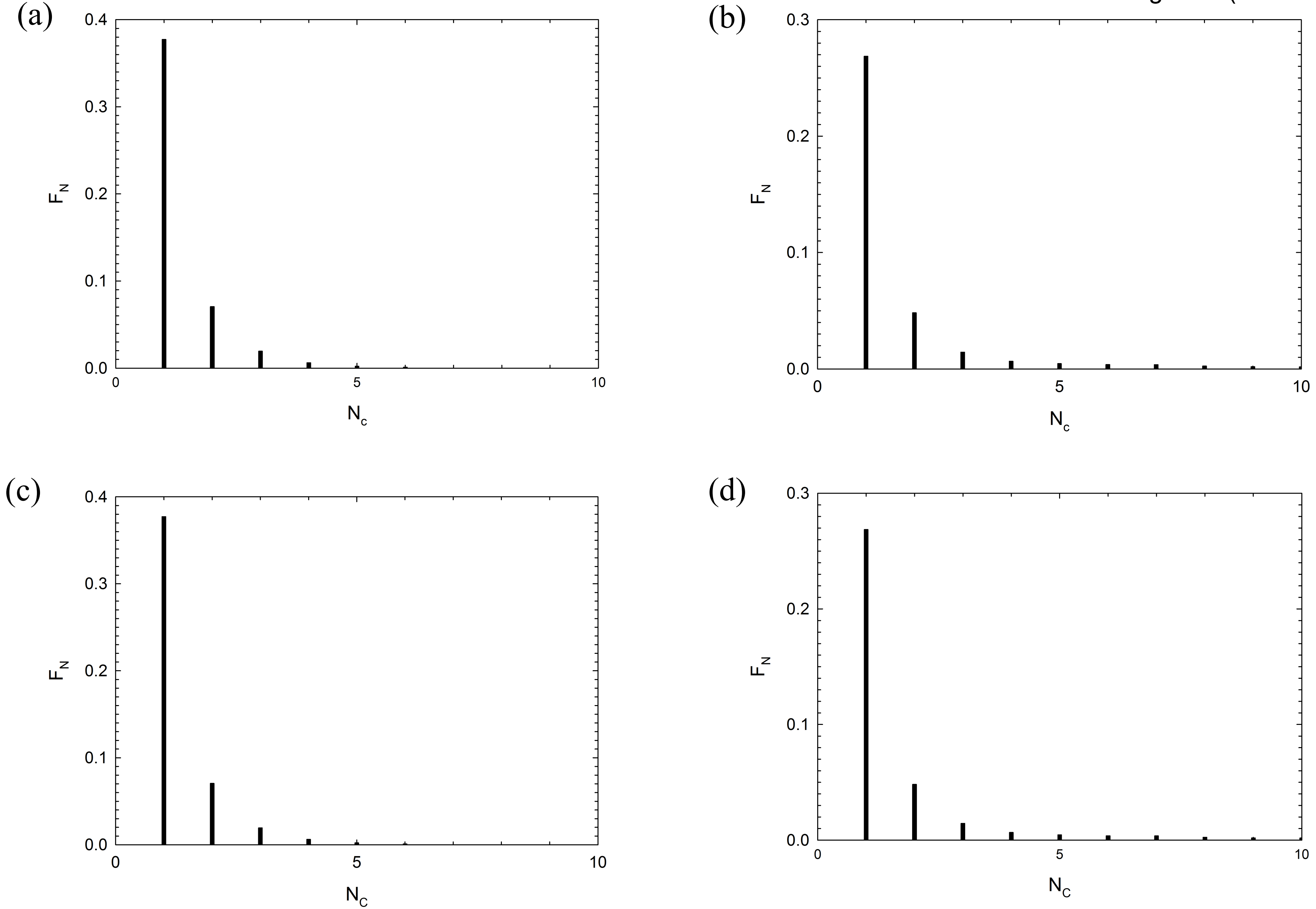

Fig. S12 (Posel et al.)